Multi#Point Observations of the Geospace Plume

Citation: Foster, J. C. et al. "Multi#Point Observations of the Geospace Plume." Geophysical Monograph Series: Dayside Magnetosphere Interactions, 248 (February 2020) © 2020 American Geophysical Union

As Published: http://dx.doi.org/10.1002/9781119509592.ch14

Publisher: Wiley

Persistent URL: https://hdl.handle.net/1721.1/125013

Version: Author's final manuscript: final author's manuscript post peer review, without publisher's formatting or copy editing

Multi-Point Observations of the Geospace Plume

J. C. Foster[1], P. J. Erickson[1], B. M. Walsh[2], J. R. Wygant[3], A. J. Coster[1], Q.-H. Zhang[4]

[1]Massachusetts Institute of Technology Haystack Observatory, Westford, MA 01886, USA

[2]Boston University, Boston MA, USA

[3]Department of Physics and Astronomy, University of Minnesota, Minneapolis, MN, USA

[4]Institute of Space Sciences, Shandong University, Weihai, Shandong, 264209, China.

Key Points:

1) Disturbance-related cold plasma redistribution in the ionosphere and magnetosphere is a unified global phenomenon, defined as the geospace plume.

2) Strong electric fields and O^+ rich plasma characterize the outer boundary of the geospace plume in the dusk sector.

3) Geospace plume ions are entrained and accelerated in reconnection exhaust jets at the dayside magnetopause.

Abstract: Simultaneous multi-instrument observations of the redistribution of cold (< 2 eV) plasma of ionospheric origin emphasize the role and importance of this system-wide phenomenon in the processes and across the regions of geospace. The geospace plume couples the ionosphere, plasmasphere, and magnetosphere from sub-auroral regions to the magnetopause, on polar field lines and into the magnetotail. We investigate the geospace plume using ground and space-based observations of the 17 March 2015 major magnetic storm. Strong electric fields, plasma waves, and accelerated heavy ions characterized Van Allen Probes observations at the source of the geospace plume in the dusk sector where energetic ring current ions overlap the outer plasmasphere. On the dayside, THEMIS spacecraft sampled the outflowing geospace plume and its involvement in reconnection at the magnetopause. Plume ions were accelerated and subsequently observed at up to ~1 keV energies in the reconnection exhaust jets.

Historical Perspective:

During major geomagnetic disturbances, cold plasma of ionospheric origin is redistributed through large portions of geospace [Freeman, 1977; Elphic et al, 1997; Foster, 2008]. Modeling the effects of **ExB** plasma motion in the outer plasmasphere, Grebowsky [1970] found that if the magnitude of the magnetospheric dawn-dusk field were suddenly increased, the plasmasphere bulge in the dusk sector would move toward the sun. Chappell [1974] reported observations of detached plasma regions outside the plasmapause and Chen and Grebowsky [1974] interpreted such observations in terms of plasmaspheric tails extending sunward in the dusk sector. Ober et al. [1997] first used the term 'plume' in describing the outflowing cold plasma. This picture was validated when space-based imagery [Sandel et al., 2001] revealed dramatic tails or drainage plumes stretching sunward from the outer plasmasphere. In situ and remote sensing space based observational studies have provided detailed characteristics of the plumes (e.g. Garcia et al. [2003]; Moldwin et al. [2004]; Darrouzet et al. [2008]). In the inner magnetosphere, cold plasma and plume phenomena are associated with the plasmasphere boundary layer (PBL) [Carpenter and Lemaire, 2004; Darrouzet et al., 2009], where cold dense material overlaps hot tenuous plasma leading to significant energy exchange and structuring.

The mid-latitude ionosphere is significantly perturbed by magnetospheric electric field effects during storms. The deep mid-latitude density trough that spans the nightside results both from sunward advection of low density plasma from the night sector and enhanced ion-neutral collisions and recombination associated with strong **ExB** plasma convection at the PBL [Schunk et al., 1976]. Penetration electric fields (e.g. Huang et al. [2005]) uplift, destabilize, and perturb the low-latitude ionosphere. Termed the dusk effect [Mendillo et al., 1970; Evans, 1970], increased storm time F-region density and total electron content (TEC) equatorward of the mid-latitude trough often are observed near sunset (e.g. Mendillo [2006] and references therein). Evans [1970] related this TEC increase to processes causing uplift of the F layer to altitudes where recombination proceeds more slowly. Evans [1973] observed a ~200 m/s westward (sunward) F region plasma drift associated with the dusk sector increase in TEC. That study concluded that horizontal transport of ionization from the evening into the afternoon sector could account for the observed increase in electron density.

Foster [1993] investigated the disturbed mid-latitude ionosphere using scanning observations with the Millstone Hill incoherent scatter radar (ISR) that provided a two-dimensional picture of ionospheric F region structure. Spatially extended sunward convecting density enhancements seen immediately equatorward of the dusk-sector ionospheric trough were termed storm enhanced density (SED). Radar-derived altitude profiles indicate that SED is characterized by a significant increase in F region scale height and peak altitude [Foster, 1993; Foster et al., 2005; Yuan et al., 2009] and occasionally with strong upward O^+ plasma velocity (> 1 km s^{-1}) in the topside F region [Yeh and Foster, 2000]. SED is observed as a continuous band (plume) of increased-density ionospheric plasma spanning a large portion of the midnight to postnoon sector (Figure 1A). The original definition of storm enhanced density by Foster [1993] was meant to describe only the enhanced ionospheric plasma streaming along the direction of the ionospheric plume at velocities of 500 to > 2000 m/s. The SED flow channel extends into the noon sector where it carries significant heavy ion fluxes into the high latitude F-region cusp ionosphere with magnitude ≥ 1.0×10^{14} m^{-2} s^{-1} [Foster et al., 2004; 2014b; Erickson et al, 2011]. In this way, a continuous stream of ionospheric plasma is carried in the SED channel from low latitudes in the evening sector to the cusp and into the polar cap at noon (Figure 1B). Detailed observations with the Poker Flat ISR have examined SED plasma characteristics in the noon sector [Zou et al., 2013]. During disturbed conditions the greatly enhanced F region density (~10x) associated with SED fluxes at the cusp provides a rich plasma source for processes accelerating ionospheric ions into the high latitude magnetosphere (e.g. the cleft ion fountain [Lockwood et al, 1985; Zeng and Horwitz, 2008] or the polar wind [Banks and Holzer, 1968; Tu et al., 2007]). Cusp outflow of ionospheric O^+ ions is believed to be the dominant source of enhanced O^+ in the storm time ring current [Kistler et al, 2016].

In the magnetosphere, O^+ of ionospheric origin appears in several energy ranges. At ~1 keV final energy, O^+ beams streaming away from a source in the cusp have been seen in the tail lobes and ultimately in the plasma sheet [Liao et al., 2010; Kistler et al, 2010]. Ionospheric O^+ outflow reaching nightside field lines can be accelerated along drift trajectories in the magnetotail, reappearing in the inner magnetosphere in the warm plasma cloak (WPC) [Chappell et al., 2008]. WPC ions are characterized by energies up to ~1 keV and distinctive bi-directional field-aligned pitch angle distributions. At energies <~ 3 keV ions accelerated earthward from the tail follow primarily eastward corotational drift trajectories, while ions ≥ 3 keV experience curvature drift westward into the pre-midnight sector. O^+ accelerated to beyond 10 keV populates the ring current [e.g. Kistler et al, 2016]. In this study, we focus on the cold (≤ 2 eV) plasma of the PBL and underlying ionosphere and trace its redistribution and involvement in processes throughout much of geospace. At these energies, plume plasma falls below the detector threshold of many particle instruments. However, cold ions can become visible to the *in situ* instruments when they are kinetically accelerated by large convection speeds such as those resulting from the motion of merged field lines as observed by Gosling et al., [1990]. In addition, low energy electron density in the plasmasphere also can be determined with active sounding instruments, like WHISPER onboard Cluster [Décréau et al., 2001; Darrouzet et al., 2013] and EMFISIS/Waves onboard Van Allen Probes [Kletzing et al., 2013 ; Kurth et al., 2015]. In this study, cold plasma density in the plume at magnetospheric altitudes is determined from spacecraft potential observations (e.g. McFadden et al. [2008b]) made with the Themis and combined spacecraft potential and EMFISIS plasma wave observations with the Van Allen Probes spacecraft (e. g. Foster et al. [2016]).

Global imaging from the ground and space has extended the two-dimensional picture of cold plume plasma redistribution at ionospheric and plasmaspheric heights. Such a geospace system perspective has been provided with distributed ground-based Global Positioning System (GPS) observations of TEC mapped to the magnetosphere equatorial plane, as shown in Figure 1D [Foster et al., 2002]. Space-based imagery of the outer plasmasphere by the IMAGE EUV instrument [Goldstein and Sandel, 2005] has provided numerous views of the structure and evolution of the erosion plume in the outer plasmaspheres (cf. Figure 1C). GPS TEC measures the integrated column content of the cold thermal electrons through the ionosphere and overlying plasmasphere to an altitude of ~20,000 km (~4 R_E) [Coster et al., 2003]. EUV images remotely sense solar 30.4-nm light that has been resonantly scattered by plasmaspheric He^+ ions, and the emission is in close correspondence to TEC in these regions [Moldwin et al, 2003]. (EUV imagery of Earth's plasmasphere has been performed from lunar orbit [Murakami et al., 2013] and with lunar-based instruments [He et al., 2016].) Combining ground and space-based plasma imaging techniques, Foster et al. [2002] demonstrated that the ionospheric SED plume was a magnetically-connected low-altitude signature of a drainage plume (plasmaspheric tail) associated with the stormtime erosion of the outer plasmasphere (Figure 1 C&D). Plasmaspheric plumes play an important role in the processes and dynamics of the inner magnetosphere where the presence of cold dense plasmaspheric ions alters the characterictics of plasma wave growth and wave-particle interactions (e.g. Chan and Holzer [1976]; Foster and Rosenberg [1976]; Summers et al. [2008]; Yuan et al. [2012a]; Foster et al. [2016]). Acceleration and loss of relativistic electrons in the outer radiation belt are strongly dependent on such wave-particle inteactions and the modulating effects of local cold plasma density (e.g Summers et al., 2007; Yuan et al., 2012b; Foster et al., 2017]).

For cold plasmas of ionospheric origin in the PBL, **ExB** redistribution entrains both low altitude ions (O^+ in the ionospheric F region) and high altitude ions (plasmaspheric and topside H^+, He^+) on the same geomagnetic flux tube. In this way, an active plume advection channel simultaneously drives horizontal ion motion at all altitudes from the ionosphere to the apex of the field lines creating a convection-defined drift shell. These plasmas convect together from the PBL to the ionospheric cusp at low altitudes and at high altitude from the dusk sector plasmaspause to the magnetopause on the dayside. At lower altitudes, the effects of dayside merging carry this large-scale plasma redistribution poleward away from the cusp into the polar cap (e.g. Zhang et al. [2013a]). A sequence of polar cap patches or an enhanced TEC tongue of ionization (TOI) results, extending anti-sunward across polar latitudes to the midnight sector auroral oval [Whitteker et al., 1976; Foster et al., 2005; Thomas et al., 2013; Zhang et al., 2013a, 2015]. Incoherent scatter radars (Sondrestrom and EISCAT) have characterized the plasmas in these polar cap plumes at altitudes below ~ 1000 km [Foster et al., 2005], while Yuan et al. [2008], using DMSP observations at ~830 km altitude, reported strong upward field-aligned plasma velocity and O^+ flux in the region where a polar TOI intersected the auroral zone near midnight. The appearance of enhanced TOI plasma density at high altitude (5.5 Re) at the midnight sector auroral oval/polar cap boundary has been reported with in situ Van Allen Probes observations [Foster et al, 2014a].

In addition to carrying a significant mass flux to the cusp ionosphere, the characteristics of SED plasma entering the polar cap across cusp latitudes provide both a tracer and signature of processes related to reconnection on cusp field lines (e.g. Zhang et al. 2015]). During disturbed conditions with an expanded polar cap, the Chatanika, Alaska ISR observed quasi-periodic bursts of enhanced topside ionospheric density streaming through the noontime cusp [Foster and Doupnik, 1984]. These observations were interpreted by Lockwood and Carlson [1992] as giving evidence that poleward convection through the cusp is pulsed with a 7- to 8-min period, consistent with the expected characteristics of transient magnetopause reconnection. The discrete nature of the F region patches in the polar cap, as reported by (e.g.) Weber et al., [1984], could be associated with such a mechanism [Zhang et al. 2013a, b].

Moore and Delcourt [1995] defined the geopause region as the volume defined by the limits of the instantaneous boundary between plasmas that are primarily of heliospheric or geospheric origin. Carpenter et al. [1993] described details of the duskside plasmasphere bulge region where outlying or outward extending plasmas are formed as products of erosion of the main plasmasphere. The study of Chandler and Moore [2003] concluded that during southward IMF periods when inner magnetosphere plasma is drawn to the dayside, the dayside boundary layer will be filled with very cold plasma drawn from the plasmasphere, and dominated in density by light ions H^+ and He^+ with densities that can be greater than 50 cm^3.This indicated an extension of the geopause to the outer edge of the magnetosphere on the dayside where cold ion densities >10 cm^{-3} could impact plasma processes and be injected into the magnetosheath on open field lines (e.g. [Zhang et al., 2018]). Plume plasmas in the outer magnetosphere are usually found in the afternoon sector with densities typically 10–100 cm^{-3} and fluxes 10^{25} to 10^{27} ions/s [Chandler et al., 1999; Moore et al., 2008; Darrouzet et al., 2008, 2009; Borovsky and Denton, 2008]. Andre and Cully [2012] found that low energy ions often dominate the magnetospheric plasma population at the dayside magnetopause with highest density and occurrence rates found in the plume drainage region in the low-latitude afternoon sector. Direct observations of the cold ions of the plasmaspheric plume have been made at the magnetopause (e.g., Walsh et al. [2013; 2014a]). Accelerated plasmaspheric plasma and ionospheric ions have been seen in reconnection-outflow fans at the dayside magnetopause by the ISEE-2 spacecraft [Gosling et al., 1990; Fuselier et al., 1991], by the Polar spacecraft [Chandler et al., 1999], and by the MPA instrument on the LANL spacecraft. Su et al. [2000] found evidence that plasmaspheric plume ions and the entering magnetosheath ions are simultaneously present on the same flux tube at the magnetopause, indicating that the plasmaspheric flux tubes are involved in dayside reconnection.

Borovsky and Denton [2008] in their statistical study of plumes at geosynchronous orbit found that about half of the outer plasmasphere is drained to the magnetopause during the first 20 hours of a storm. Modeling studies by Elphic et al. [1997] described the transport of outer plasmasphere flux tubes from the dayside, over the polar cap and into the magnetotail. Su et al. [2001a] interconnected ionospheric observations of SED with plasmaspheric tails and the large-scale redistribution of cold plasma in the magnetosphere. Accelerated plasmaspheric plasma has been seen over the polar cap by both the Interball and the Polar spacecraft [Su et al., 2001b]. Foster et al. [2014a] reported spacecraft potential observations of cold TOI plasma at 5 R_E altitude on field lines mapping to the region where the trans-polar cap TOI intersected the auroral oval in the midnight sector.

Observational Synthesis: The Geospace Plume

Previous studies have developed the picture of the redistribution of cold plasma from the ionosphere and inner magnetosphere to the cusp, magnetopause, polar cap, and into the nightside auroral ionosphere – i.e. throughout a large portion of geospace. By necessity, these results have been presented in a gradually evolving fashion over time based largely on increased capabilities of ground-based and space-based imaging, modeling, and in situ observations. Moldwin et al. [2016] provided a synthesis of recent literature describing appearance of plumes in different measurements in different regions and concluded that those structures are either directly related to or connected in the causal chain of plasma redistribution throughout the magnetosphere-ionosphere system. Plumes serve to describe an emerging conceptual framework of the flow of high-density–low-latitude ionospheric plasma into the magnetosphere. The nomenclature describing the various aspects of the plume phenomena is varied according to feature identification and scope, and is largely dependent on the characteristics and location of the separate measurements. We propose the recognition of disturbance-related cold plasma redistribution as a unified global phenomenon – the geospace plume. Its wide spatial extent from sub-auroral regions, to the cusp and the magnetopause, on polar field lines, and into the magnetotail characterizes the system-wide coupling of the ionosphere, plasmasphere, and magnetosphere. In the following sections, we describe how the geospace plume manifests itself in different regions of the ionosphere-magnetosphere system.

Geospace Plume Features at Disturbance Times

We describe a recent disturbance event with near simultaneous observations of the plume in multiple regions of geospace in order to demonstrate the characteristics and continuity of the geospace plume through the coupled ionosphere-magnetosphere system. The event also provides insight into dynamic features of the geospace plume.

One of the largest geomagnetic disturbances of the past decade began with the arrival of a solar wind shock at Earth and storm sudden commencement at ~04:45 UT on 17 March 2015. A full description of this storm interval has been provided by Baker et al. [2016]. Other related studies of this storm include those by Goldstein et al. [2017] and Runov et al. [2016]. Figure 2 presents an overview of solar wind and magnetospheric responses during 17-18 March 2015 from 1-min cadence observations in the NOAA OMNI database. A solar wind shock and storm sudden commencement occurred at ~04:45 UT on 17 March while Bz was positive. Solar wind speed V_{SW} (not shown) increased from V_{SW} ~ 400km/s to V_{SW} ~ 500 km/s after the shock passage while the total magnetic field $|B_{SW}|$ (not shown) increased from ~10 nT to > 25 nT. After 12:00 UT Bz turned strongly southwards (Bz ~ 20 nT), V_{SW} increased to ~ 600 km/s, and solar wind dynamic pressure P_{SW} exceeded 30 nPa. As the main storm phase began and SYM-H was decreasing, there was a 2-hour gap in the ACE solar wind H+ density, velocity, and magnetic field data where P_{SW} cannot be determined. Minimum SYM-H reached < -220 nT at ~23:00 UT on 17 March and by early on 18 March the plasmasphere had been eroded to L ~ 1.9 [Foster et al., 2016]. During the event, the orbital coverage of the Van Allen Probes twin spacecraft (also called Radiation Belt Storm Probes (RBSP), [Mauk et al, 2013]) was well aligned to provide near-equatorial in situ observations (Figure 3) at the source of the plume (i.e its point of attachment to the plasmasphere in the dusk sector PBL [Darrouzet et al., 2006; Coster et al., 2007]) . At the same time the three THEMIS spacecraft [Angelopoulos, 2008] probed the dayside extension of the plume from the plasmasphere to the magnetopause where the cold plume ions were observed to be involved in magnetic reconnection. Ground-based five-minute median values of GPS TEC at 350-km altitude ionospheric penetration points were accumulated on a 1 deg by 1 deg latitude/longitude grid [Rideout and Coster, 2006]. The ionospheric footprint of the TEC observations was projected into the magnetospheric equatorial plane along magnetic field lines using the Tsyganenko 2004 magnetic field model [Tsyganenko and Sitnov, 2005]. Excellent coverage of the spatial extent and development of the SED signature of the plume at ionospheric altitudes was simultaneously provided by the Millstone Hill incoherent scatter radar, global GPS TEC mapping, and the DMSP satellites [Strom and Iwanaga, 2005] crossing auroral and polar latitudes at dusk and dawn in sun-synchronous orbits at

~830 km altitude. This array of space and ground-based instruments provided continuing coverage of the formation and evolution of the plume throughout the event. Here we concentrate on an interval of simultaneous observations during the main phase of the storm near 16:00 UT on 17 March 2015 when IMF B_Z was strongly negative (~ -20 nT) and Dst was decreasing (cf. Figure 2) and a strong plume was evolving.

Geospace Plume Source: SAPS and Plasmasphere Erosion

The geospace plume has its origins on inner magnetospheric fields lines in the pre-midnight and dusk sector. During disturbed conditions at the PBL an electric shielding layer is set up at the location where the freshly injected ring current particles abut the plasmapause. The inward extent of the energetic ring current ions lies earthward of the plasma sheet electrons. Region II currents are driven into the sub-auroral ionosphere where a strong poleward electric field is set up to drive Pedersen closure currents in the low conductivity ionosphere equatorward of precipitating auroral electrons. This sub-auroral polarization stream electric field (SAPS [Foster and Burke, 2002]) overlaps the outer plasmasphere and draws out the SED/plasmasphere erosion plumes that stretch sunward from their dusk-sector source to the dayside cusp in the ionosphere and to the magnetopause merging region [Foster et al., 2002; 2004; 2007; 2014b]. During the 17 March 2015 event, Van Allen Probe A, at 18 MLT and 3 R_E altitude, was well positioned to observe the ring current, the SAPS electric field, and the sunward transport of the geospace plume in the SAPS channel in the inner magnetosphere (Figure 4). (Van Allen Probe B made a similar encounter with the plume and the PBL some 5 hours later during the event.) Observations with the Electric Field and Waves instrument (EFW [Wygant et al., 2013]) measured the electric field and in situ density across the SAPS channel (Figure 4 A, B; electric fields are presented in magnetic field aligned coordinates). The dominant radially outward electric field component (~ 10 mV/m; shown in red) drove strong sunward convection in the geospace plume consistent with statistical studies of the SAPS convection flow [Foster and Vo, 2002].

Ion composition and spectra were observed across the outer plasmasphere, PBL, and geospace plume with the HOPE instrument on the Van Allen Probes spacecraft [Funsten et al, 2013]. A 'nose' of hot ring current O^+ ions (e.g. Smith and Hoffman [1974]) extended across the region of SAPS electric field (Figure 4 C). During these disturbed conditions, fluxes of O^+ ions with bi-directional field-aligned pitch angle distribution were observed immediately adjacent to the outer extent of the geospace plume at energies below and up to ~ 10 keV. Figure 4 (Panels C and D) present observations of these O^+ ions and their field-aligned pitch angle distribution at 7 keV. Although this energy is quite high with respect to previous discussions of the WPC, the pitch angles and O^+/H^+ density ratio (~ 1) of these ions are suggestive of the dusk sector WPC as described by Chappell et al. [2008].

Plasma Redistribution in the Ionosphere

At ionospheric heights, the SAPS channel plays a key role in carrying the geospace plume to the cusp where F-region plume plasma enters the polar cap on reconnecting flux tubes. During the 17 March 2015 event, the redistribution of cold ionospheric plasma was observed in multiple locations with the Millstone Hill incoherent scatter radar and DMSP low-altitude satellites (Figure 5). Shortly after 16:00 UT the radar scanned to the north and west across the local noon sector (Panel 5A) and at 16:14 UT (68^o maglat, ~11 MLT) observed plume plasma at 500 km altitude streaming into the cusp and polar cap with ~1000 m/s flow speed (Panel 5B). The spatial distribution and temporal variation of plume plasma entering the polar cap identifies the ionospheric footprints of reconnecting field lines at the magnetopause (e.g. Zhang et al. [2013a]). At sub-auroral latitude, DMSP at 840 km altitude (16:15 UT, ~16 MLT, 57^o maglat) crossed the SAPS/SED region sampled by Van Allen Probe A (cf. Figure 4) and shortly thereafter (16:24 UT; Panel 5C) intersected the plume plasma in the center of the northern polar cap. Plasma flow velocity > 1500 m/s was observed in the dusk sector SAPS channel by the DMSP drift meter (Panel 5D) at the location where a distinct density enhancement delineated the signature of the geospace plume in the topside ionosphere. (Foster et al. [2014b] provided a detailed examination of a similar conjunction between Van Allen Probes and DMSP crossings of the SAPS and plume in the dusk sector during the 17 March 2013 storm event.)

Later in its orbit, DMSP F-16 clearly observed the anti-sunward transport of geospace plume plasma in the center of the polar cap. Here magnetic field lines map into the magnetotail lobes and the motion of patches, blobs, and TOI plasma reflect the transport of the geospace plume from the dayside merging region into the magnetospheric tail [Zhang et al., 2016]. A regular variation of the anti-sunward plasma flow velocity from ~500 m/s to ~ 1000 m/s was observed as DMSP F-16 crossed polar latitudes from dusk to dawn. Plume plasma largely was confined to the dusk side of the polar region.

Observations of the Geospace Plume in the Dayside Magnetosphere

During the 17 March 2015 event the orbits of the THEMIS spacecraft intersected the plume at radial distances of 4 to 7 R_E in the noon sector (cf. Figure 3) providing excellent measurements of plume characteristics in the outer magnetosphere as it was transported sunward in the SAPS flow. The three THEMIS spacecraft (A, E, and D) traveled along the same orbit and sequentially sampled (with ~2-hr separation) the outflowing geospace plume and its appearance in the reconnection region at the magnetopause. Figure 6 presents THEMIS-A observations along its outbound orbit near 16 UT. The spacecraft exited the morning sector plasmasphere at ~14:40 UT and entered the plume near 15:40 UT. Cold plasma density determined from spacecraft potential values was ~ 100 cm^{-3} within the dayside plume, with lower densities ~10–40 cm^{-3} adjacent to reconnection sites at the magnetopause. Warm plasma density ~60 cm^{-3} (ESA ion measurements, not shown) was observed in the magnetosheath beyond the reconnection region.

Reconnection: The next step in the circulation of the geospace plume on this day was observed at the magnetopause where its cold dense plasma was seen to participate in magnetic reconnection. As THEMIS-A traveled outward, it encountered the magnetopause a number of times beginning near 16:00 UT and crossed into the magnetosheath for the final time at 16:29 UT (cf. Figure 6). At each magnetopause encounter, several signatures demonstrated active magnetic reconnection and the participation of cold plasma in the process. High velocity reconnection exhaust jets, primarily in the Z-direction (measured with the ESA detector, black curve in Panel B), accompanied a +/- rotation in the Z component of the magnetic field (not shown). The magnitude of the jet velocity is consistent with theoretical predictions for asymmetric reconnection [Cassak and Shay, 2007]. That theory predicts an outflow jet velocity of 352 km/s for the boundary parameters at 16:29 UT. At 16:29 UT (arrow on Panel B) the spacecraft measured a jet of 343 km/s in the reconnecting component, consistent with (97% of) the prediction.

Associated with the reconnection exhaust jets, cold plasma (< 3 eV) was accelerated into the observational range of the ESA ion detector and appeared as distinct ion populations at the appropriate kinetic energy for both protons and helium. Immediately outside the reconnection line (cf. at 16:00 UT) a mixture of magnetosheath and accelerated cold ions was observed with a combined warm plasma density ~100 cm^{-3}.

Details of the plasma distributions observed as THEMIS-A crossed the reconnection region from the magnetosphere into the magnetosheath near 16:17:30 UT are presented in Figure 7. Panel A presents ion energy flux observations over a ~ 3 min interval as the fluctuating magnetopause position carried the merging region back and forth over the outbound spacecraft. Panel B presents observations of cold plasma density calculated from spacecraft potential (blue), the Z_{GSM} component of the magnetic field (red; positive in magnetosphere, negative in the magnetosheath), and the field aligned velocity (black; Vz) identifying high-speed flows in the reconnection jets. Sequentially, the instruments sampled the magnetosheath (16:16:30 UT), the reconnection exhaust jet (16:17:00 UT), magnetospheric plasma populations immediately earthward of the merging region (16:17:30 UT), the merging region and exhaust jet (16:18:10 UT), and finally the magnetosheath (16:18:40 UT). Cold ions (~10 cm^{-3}) calculated from the spacecraft potential were observed immediately adjacent to the reconnection region (blue curve in Panel B). A pronounced low energy population with center energy ranging from <5 eV to ~50 eV was seen (Panel A) in the magnetospheric region between 16:17 UT and 16:18 UT. Although the energy of cold plume ions falls below the minimum detector threshold of the THEMIS ESA instrument (~ 5 eV), the kinetic energy of the cold population can be increased into the detectable energy range during times of strong flows [Gosling et al, 1990; McFadden et al. 2008a,b; Andre and Cully, 2012; Lee and Angelopoulos, 2014]. Such acceleration and/or heating can occur when cold ions become involved in the reconnection processes [Zhang et al., 2018]. The effects of cold ion acceleration are seen in Panel A around 16:17:15 UT and again near 16:17:50 UT when the sharply defined low energy population was observed with increasing central energy at progressively closer distances to the edge of the reconnection jet.

Velocity distributions for the ion populations observed in this region are shown in Figure 8. The magnetospheric ion populations immediately adjacent to the magnetopause were observed at 16:17:35 UT (panel A). A weak flux of the cold plume ions was seen above detector threshold around zero energy, surrounded by a halo of warm magnetospheric ions. Panels B presents four successive 3-s velocity distributions observed as THEMIS-A approached the magnetopause and the merging region. The cold ion flux above detector threshold increased by >100x and the energetic magnetosheath ions appeared at higher energies. ESA ion energy distributions shown in panel C identify the magnetosheath population near 1 MeV. Kinetic signatures of reconnection are observed in the particle distribution. Clear "D-shaped" ion distributions, representative of the reflected and transmitted magnetosheath particles on newly opened field lines [Cowley 1982], are observed (panel B frames 110 and 111). A portion of the cold population is progressively kinetically accelerated to > 300 eV energy as the exhaust jet was entered at 16:18:00 UT (cf Figure 7). The progressively increasing peak energies of the low energy ion peak in panel C correspond to the kinetic energies of H^+ ions for the observed values of V_Z as shown in Figure 7. The significant ion fluxes observed at energies below the cold ion peak indicate that not all of the cold ion population in this region had gained the full jet flow velocity parallel to the magnetic field. Rather, a population of ions that had picked up the ExB drift of the boundary layer also was being seen. The THEMIS observations at the magnetopause during this event demonstrate the complexities and intermingling of the cold, warm, and accelerated ion populations that characterize this dynamic region.

In the following, we compare the cold magnetospheric ion population identified as geospace plume plasma in the above discussion with cold plasma characteristics directly measured in the outer plasmasphere at L ~ 4 during a previous event. In Figure 9A we show the one-dimensional THEMIS-A ion energy distribution cutting across the low energy population at 16:17:15 UT (black vertical line in Figure 7). Although there is no mass discrimination in the THEMIS ESA detectors, the difference in the kinetic energies of cold ion species accelerated in the outer regions of the reconnection velocity field produces clearly separated H^+ and He^+ energy peaks. We note that here, on the edge of the merging region, these cold species appear on the same field lines with magnetosheath ions at higher energies > 2 keV. The larger gyroradii of the more energetic magnetosheath ions results in their incursion onto field lines associated with the guiding centers of the adjacent colder population. Following the method described by Sauvaud et al. [2001], we find the temperature of this cold H^+ population to be ~3 eV, as calculated from the energy spread of its 1-D distribution (Panel B). The ~ 13 eV central energy of the H^+ peak corresponds to the kinetic energy of a population of H^+ ions in the ~65 km/s velocity field observed at this position. The ~3 eV temperature for the H^+ ions observed at the merging region is consistent with ion temperatures in the outer plasmasphere at L ~ 4 as has been observed with the Van Allen Probes HOPE ion spectrometer. This consistency is highlighted in Panel C where we plot the spectral widths of H^+ and He^+ ions accelerated kinetically to energies greater than the ~ 2 eV HOPE energy threshold by strong storm-induced ULF waves during the shock-induced storm of 8-9 October 2013 [Foster et al., 2015]. The RBSP-A spacecraft was well inside the dusk side plasmapause at the time. Plasmaspheric H^+ and He^+ temperatures near the apex of magnetic field lines in the PBL for this separate event were 1.5 eV and 2.5 eV, fully consistent with the temperature of the low energy ion population described in Panel B. Comparing the spectral peaks across the two different events in Panels A and C, we note that the H+/He+ flux ratio was ~20 in the outer plasmasphere (Panel C) and ~ 40 in the plume at the dayside magnetopause (Panel A). THEMIS-A ESA observations of warm (i.e. > 5 eV) ion density (not shown) in the magnetospheric plasma region of Figure 7 Panel A (16:17:40 UT) were at ~ 1 cm^{-3} levels. Cold plasma density observed by spacecraft potential was significantly larger, varying from 10 - 40 cm^{-3} in these regions. As the cold ions were accelerated kinetically into the energy range of the ESA detector and began to contribute to the warm ion density, the ion density determined by the ESA instrument increased to ~ 40 cm^{-3} in regions where no magnetosheath ions were being observed. We note that it is probable that additional ion sources also can be involved in reconnection (e.g. the low energy component of warm plasma cloak ions reported at the dayside magnetopause by Chappell et al. [2008]). Significantly, for the 17 March 2015 event discussed here, the density, temperature, and ion composition of the low energy ions at the magnetopause are consistent with those of the geospace plume. We conclude that, during this event, geospace plume ions were accelerated and entrained into the reconnection exhaust jets at the dayside magnetopause.

These observations give strong evidence that the cold ionospheric source plasma of the geospace plume can be directly involved in dayside reconnection. In previous studies, these dense populations of cold ionospheric/plasmaspheric material have been shown to have a significant impact on the efficiency and structure of reconnection processes (e.g. Walsh et al., [2013, 2014a, b]; Lee et al. [2014]; Wang et al. [2014]; Toledo-Redondo [2015]; Zhang et al. [2018]). The newly reconnected field lines are carried anti-sunward into the tail lobe and over the pole, carrying the geospace plume plasma with them at both ionospheric and magnetospheric altitudes. At the ionospheric footprint of these field lines, the geospace plume is seen as the tongue of ionization (e.g. Whitteker et al. [1976]; Foster et al. [2005]) or polar cap patches (e.g. Weber et al. [1984]; Zhang et al. [2013b]) that are carried to the nightside auroral oval in the anti-sunward flow across the polar cap [Foster et al., 2005; Zhang et al., 2015]. This polar region plasma transport is observed in both the ionosphere and at magnetospheric altitudes. Foster et al. [2014a] have reported the observation at 5 R_E altitude in the near magnetotail of cold plume plasma on field lines mapping to the point where the TOI intersected the auroral oval in the midnight sector.

Plasma flux: The system-wide redistribution of cold ionospheric-plasmaspheric ions associated with the geospace plume has been presented through a synthesis of observations made with a variety of instruments. The Van Allen Probes and THEMIS spacecraft carry a full complement of instruments characterizing electric field, velocity, cold plasma density, magnetic field, ion and electron energy and pitch angle distributions. We obtained measurements of plasma density and flow velocity (either directly or from **E**x**B**) for all observing sites, allowing calculation of the plasma flux (velocity * density) within the plume at multiple points (observations for the 17 March 2015 event are shown in Table 1). Prior observations of plasma flux in the geospace plume at ionospheric heights [Foster et al., 2004; Erickson et al., 2011] have been reported with values ~ 1.e14 $m^{-2}s^{-1}$ for transport toward the cusp, in good agreement with these observations. For the 17 March 2015 event, analysis of THEMIS ESA ion spectra and velocities at the magnetopause yield an observation of ~ 1.e13 $m^{-2}s^{-1}$ for the flux of accelerated plume ions entrained in the reconnection exhaust jets. In their statistical study of Cluster observations, Andre and Cully [2012] estimated low energy ion outflow at the magnetopause for their strongest plume events > 10^{27} ions s^{-1}. Projecting ionospheric observations of plume plasma flux into the outer plasmasphere, Foster et al. [2004] estimated a total sunward flux of > 10^{27} ions s^{-1}.

Discussion: The 17 March 2015 event provides a well-observed example of the very good correspondence between the positions and dynamics of the geospace plume observed both at low altitudes and with *in situ* observations at magnetospheric heights. Recently Krall et al. [2018], using SAMI3 simulations to investigate a long-lived magnetospheric plume, found that high-speed, field-aligned plasma flows from the ionosphere contribute significantly to plume density. We find that boundaries, features and dynamics of ground-based TEC observations associated with the redistribution of plasma (TEC) at ionospheric heights map to similar characteristics of the plume at magnetospheric altitudes. We note that the magnitude of the TEC shown in the equatorially projected ionospheric maps should not be construed as a direct measurement of the absolute or relative value of the plume plasma density at the apex of the field lines. The ~4 R_E orbital location of GPS satellites limits the extent of their coverage to the ionosphere and near-earth magnetosphere. In addition, most of the integrated TEC content is found to lie below ~ 1000 km altitude (e.g. as shown in Foster et al. [2014b], Figure 3). However, while the absolute magnitude of the TEC is controlled primarily by lower altitude processes in the ionosphere and thermosphere, the structure and dynamics of the geospace plume as revealed in the TEC images provides an excellent indication of boundaries in the coupled ionosphere – magnetosphere system, and illuminates the overall transport of the cold geospace plume plasma throughout the system.

We suggest that the geospace plume has significant effects throughout the coupled geospace system. The details and processes associated with these effects provide ample opportunities for further investigation. These include:

- Redistribution of plume plasma to the dayside magnetopause and its subsequent effects on reconnection;
- Plume plasma as a potential source for heavy ions in the magnetosphere through processes occurring both in the topside cusp ionosphere and at the magnetopause merging region;

- Contribution made by plume plasma to the particle populations accelerated into the plasmasheet and ring current during substorm injections;
- Cold plasma modification of wave-particle interactions in the magnetosphere, with subsequent effects on energetic particle populations.

We have found that a multiplicity of aspects of cold plasma redistribution are interconnected and are manifestations of the geospace plume that threads and interconnects regions and processes throughout much of Earth's plasma environment. Adoption of a common nomenclature for this system-wide phenomenon accentuates the coupling that underlies geospace processes and characteristics.

Acknowledgments: JCF and PJE received support from a U. Minn. subcontract award to the Massachusetts Institute of Technology. Van Allen Probes data access was provided through the Johns Hopkins University/Applied Physics Lab Mission Operations Center and the Los Alamos National Laboratory Science Operations Center. This work was supported by JHU/APL contract 967399 under NASA's prime contract NAS5-01072. All Van Allen Probes data used are publicly available at (www.rbsp-ect.lanl.gov). The authors wish to thank the International Space Science Institute in Beijing (ISSI-BJ) for supporting and hosting the meetings of the International Team on "Multiple-instrument observations and simulations of the dynamical processes associated with polar cap patches/aurora and their associated scintillations", during which discussions contributing to this publication were held.

REFERENCES

André, M., and C. M. Cully (2012), Low-energy ions: A previously hidden solar system particle population, *Geophys. Res. Lett*., *39*, L03101, doi:10.1029/2011GL050242.

Angelopoulos, V. (2008), *Space Sci. Rev*., 141: 5, 5-34. https://doi.org/10.1007/s11214-008-9336-1.

Banks, P. M., and T. E. Holzer (1968), The polar wind, *J. Geophys. Res., 73(21*), 6846–6854, doi:10.1029/JA073i021p06846.

Baker, D. N., et al. (2016), Highly relativistic radiation belt electron acceleration, transport, and loss: Large solar storm events of March and June 2015, *J. Geophys. Res. Space Physics, 121*, 6647-6660, doi:10.1002/2016JA022502.

Borovsky, J. E., and M. H. Denton (2008), A statistical look at plasmaspheric drainage plumes, *J. Geophys. Res.*, *113*, A09221, doi:10.1029/2007JA012994.

Carpenter, D. L., and J. Lemaire (2004), The plasmasphere boundary layer, *Ann. Geophys., 22*, 4291-4298, https://doi.org/10.5194/angeo-22-4291-2004.

Carpenter, D. L. et al. (1993), Plasmasphere dynamics in the duskside bulge region: A new look at an old topic, *J. Geophys. Res., 98(A11)*, 19243–19271, doi:10.1029/93JA00922.

Cassak, P. A. and M. A. Shay (2007), Scaling of asymmetric magnetic reconnection: General theory and collisional simulations, Phys. Plasmas, 14, 102-114, doi:10.1063/1.2795630 .

Chan, K. W., and R. E. Holzer, 1976. ELF hiss associated with plasma density enhancements in the outer magnetosphere, J. Geophys. Res. , 81 (13), 2267-2274, doi: 10.1029/JA081i013p02267.

Chandler, M. O., and T. E. Moore (2003), Observations of the geopause at the equatorial magnetopause: Density and temperature, *Geophys Res. Lett.*, 30 (16), 1869, doi: 10.1029/2003GL017611.

Chandler, M. O., et al. (1999), Evidence of component merging equatorward of the cusp, *J. Geophys. Res., 104*, 22623-22633, doi:10.1029/1999JA900175.

Chappell, C. R. (1974), Detached plasma regions in the magnetosphere, J. Geophys. Res., 79, 1861-1870, doi:/10.1029/JA079i013p01861.

Chappell, C. R., M. M. Huddleston, T. E. Moore, B. L. Giles, and D. C. Delcourt (2008), Observations of the warm plasma cloak and an explanation of its formation in the magnetosphere, *J. Geophys. Res., 113*, A09206, doi:10.1029/2007JA012945.

Chen, A. J., and J. M. Grebowsky (1974), Plasma tail interpretations of pronounced detached plasma regions measured by OGO 5, J. Geophys. Res., 79, 3851–3855, doi:10.1029/JA079i025p03851.

Cowley, S. W. H. (1982), The causes of convection in the Earth's magnetosphere: a review of developments during the IMS, *Rev. Geophys. Space Phys.*, *20*, 531-565, doi:10.1029/RG020i003p00531.

Coster, A. J., J. Foster, and P. Erickson (2003), Monitoring the ionosphere with GPS: Space weather, GPS World, 14(5), 42–49.

Coster, A. J., et al. (2007), Longitude sector comparisons of storm enhanced density, *Geophys. Res. Lett.*, *34*, L18105, doi:10.1029/2007GL030682.

Darrouzet, et al. (2008), Statistical analysis of plasmaspheric plumes with CLUSTER/WHISPER observations, *Ann. Geophys.*, *26 (8),* 2403–2417, doi:10.5194/angeo-26-2403-2008.

Darrouzet, F., et al. (2009), Plasmaspheric density structures and dynamics: Properties observed by CLUSTER and IMAGE missions, *Space Sci. Rev.*, *145*(*1-2*), 55-106, doi:10.1007/s11214-008-9438-9.

Darrouzet, F., et al. (2006), Analysis of plasmaspheric plumes: CLUSTER and IMAGE observations, *Ann. Geophys.*, *24*, 1737-1758, https://doi.org/10.5194/angeo-24-1737-

2006.

Darrouzet, F., et al. (2013), Links between the plasmapause and the radiation belt boundaries as observed by the instruments CIS, RAPID and WHISPER onboard Cluster, J. Geophys. Res. Space Physics, 118, 4176–4188, doi:10.1002/jgra.50239.

Décréau, P. M.E., et al. (2001), Early results from the Whisper instrument on Cluster: an overview, Ann. Geophys., 19 (10-12), 1241–1258, doi:10.5194/angeo-19-1241-2001.

Elphic, R. C., et al. (1997), The fate of the outer plasmasphere, *Geophys. Res. Lett., 24,* 365-368, doi:10.1029/97GL00141.

Erickson, P. J., F. Beroz, and M. Z. Miskin (2011), Statistical characterization of the American sector subauroral polarization stream using incoherent scatter radar, J. Geophys. Res., 116, A00J21, doi:10.1029/2010JA015738.

Evans, J. V. *(*1970*),* The June 1965 magnetic storm: Millstone Hill observations*,* J. Atmos. Terr. Phys.*,* 32*,* 1629–1640, https://doi.org/10.1016/0021-9169(70)90169-8.

Evans, J. V. (1973), The causes of storm-time increases of the F layer at mid-latitudes, J. Atmos. Terr. Phys., 35, 593-616, https://doi.org/10.1016/0021-9169(73)90191-8.

Foster, J. C. (1993), Storm-time plasma transport at middle and high latitudes, *J. Geophys. Res., 98,* 1675-1689, doi:10.1029/92JA02032.

Foster, J. C. (2008), Ionospheric-magnetospheric-heliospheric coupling: Stormtime thermal plasma redistribution, in *Mid-Latitude Dynamics and Disturbances*, Geophys. Monograph Ser. 181, Am. Geophys. Union, 10.1029/181GM12.

Foster, J. C., and W. J. Burke, (2002). SAPS: A new characterization for sub-auroral electric fields, EOS, 83, 393-394, https://doi.org/10.1029/2002EO000289.

Foster, J. C. and J. R. Doupnik (1984), Plasma convection in the vicinity of the dayside cleft, *J. Geophys. Res., 89,* 9107-9113, doi:10.1029/JA089iA10p09107.

Foster, J. C.*,* and T. J. Rosenberg *(*1976*),* Electron precipitation and VLF emissions associated with cyclotron resonance interactions near the plasmapause*, J. Geophys. Res., 81(13),* 2183–2192*, doi:*10.1029/JA081i013p02183

Foster, J. C., and H. B. Vo (2002) Average characteristics and activity dependence of the subauroral polarization stream, *J. Geophys. Res*., *107(A12*),1475, doi: 10.1029/2002JA009409.

Foster, J. C., et al. (2002), Ionospheric signatures of plasmaspheric tails, *Geophys. Res. Lett., 29*(13), 10.1029/2002GL015067.

Foster, J. C., et al. (2004), Stormtime observations of the flux of plasmaspheric ions to the dayside cusp/magnetopause, *Geophys. Res. Lett., 31*, L08809, doi:10.1029/2004GL020082.

Foster, J. C., et al. (2005), Multiradar observations of the polar tongue of ionization, *J. Geophys. Res.*, 110, A09S31, doi:10.1029/2004JA010928.

Foster, J. C., et al. (2007), On the relationship of SAPS to storm enhanced density, *J. Atmos. Space Terr. Phys.,* 69, 303-313, https://doi.org/10.1016/j.jastp.2006.07.021.

Foster, J. C., et al. (2014a), Prompt energization of relativistic and highly relativistic electrons during substorm intervals: Van Allen Probes observations, *Geophys. Res. Lett.*, 41, 20-25, DOI: 10.1002/2013GL058438

Foster, J. C., et al. (2014b), Stormtime observations of plasmasphere erosion flux in the magnetosphere and ionosphere, *Geophys. Res. Lett,* 41, 762-768, DOI: 10.1002/2013GL059124.

Foster, J. C., J. R. Wygant , M. K. Hudson, A. J. Boyd, D. N. Baker, P. J. Erickson, and H. E. Spence (2015), Shock-Induced Prompt Relativistic Electron Acceleration in the Inner Magnetosphere, *J. Geophys. Res.*, 120, doi: 10.1002/2014JA020642.

Foster, J. C., et al. (2016), Observations of the impenetrable barrier, the plasmapause, and the VLF bubble during the 17 March 2015 storm, *J. Geophys. Res. Space Physics, 121, 5537–5548*, doi:10.1002/2016JA022509.

Foster, J. C., et al. (2017), Van Allen Probes Observations of Prompt MeV Radiation Belt Electron Acceleration in Non-Linear Interactions with VLF Chorus, *J. Geophys. Res. Space Physics,* doi: 10.1002/2016JA023429.

Freeman, J. W. (1977), Heavy ion circulation in the Earth's magnetosphere, Geophys. Res. Lett., 4, 195-197, doi:10.1029/GL004i005p00195.

Funsten, H. B., et al. (2013), Helium, Oxygen, Proton, and Electron (HOPE) mass spectrometer for the Radiation Belt Storm Probes Mission, *Space Sci. Rev., 179*, 423–484, doi:10.1007/s11214-013-9968-7.

Fuselier, S. A., et al. (1991), Ion reflection and transmission during reconnection at the Earth's subsolar magnetopause, Geophys. Res. Lett., 18, 139-142, doi:10.1029/90GL02676.

Garcia, L. N., et al. (2003), Observations of the latitudinal structure of plasmaspheric convection plumes by IMAGE-RPI and EUV, *J. Geophys. Res.*, *108 (A8)*, 1321-1332, doi:10.1029/2002JA009496.

Goldstein, J., and B. R. Sandel (2005), The global pattern of evolution of plasmaspheric drainage plumes, pp 1-22, in *Inner Magnetosphere Interactions: New Perspectives from Imaging*, J. Burch and M. Schultz, eds., AGU Press, Washington, DC, DOI: 10.1029/159GM02.

Goldstein, J., et al., (2017), Cross-scale observations of the 2015 St. Patrick's day storm: THEMIS, Van Allen Probes, and TWINS,J. Geophys. Res. Space Physics, 122, 368–392, doi:10.1002/2016JA023173.

Gosling, J. T., et al. (1990), Cold ion beams in the low latitude boundary layer during accelerated flow events, Geophys. Res. Lett., 17, 2245-2248, doi:10.1029/GL017i012p02245.

Grebowsky, J. M. (1970), Model study of plasmapause motion, *J. Geophys. Res., 75,* 4329, doi:10.1029/JA075i022p04329.

He, F., et al. (2016), Determination of the Earth's plasmapause location from the CE-3 EUVC images, J. Geophys. Res. Space Physics, 121, 296–304, doi:10.1002/2015JA021863.

Huang, C.S., J. C. Foster, M. C. Kelley (2005), Long-duration penetration of the interplanetary electric field to the low-latitude ionosphere during the main phase of magnetic storms, *J. Geophys. Res., 110*, A11309, doi:10.1029/2005JA011202.

Kistler, L. M., et al. (2010), Cusp as a source for oxygen in the plasma sheet during geomagnetic storms, *J. Geophys. Res., 115*, A03209, doi:10.1029/2009JA014838.

Kistler, L. M.*, et al. (*2016*),* The source of O^+ in the storm time ring current*, J. Geophys. Res. Space Physics*, 121, 5333–5349, doi:10.1002/2015JA022204.

Kletzing, C. A., et al. (2013), The Electric and Magnetic Field Instrument Suite and Integrated Science (EMFISIS) on RBSP, Space Sci. Rev., 179 (1–4), 127–181, doi:10.1007/s11214-013-9993-6.

Krall, J., J. D. Huba, and J. E. Borovsky (2018), SAMI3 simulations of a persistent plasmasphere plume, *Geophys. Res. Lett*., *45*, https://doi.org/10.1002/2017GL076448.

Kurth, W. S., et al. (2015), Electron densities inferred from plasma wave spectra obtained by the Waves instrument on Van Allen Probes, J. Geophys. Res.Space Physics, 120 (2), 904–914, doi:10.1002/2014JA020857.

Lee, S. H., et al. (2014), Plasma and energetic particle behaviors during asymmetric magnetic reconnection at the magnetopause, *J. Geophys. Res. Space Physics*, 119, doi:10.1002/2013JA019168.

Lee, J. H., and V. Angelopoulos (2014), On the presence and properties of cold ions near Earth's equatorial magnetosphere, *J. Geophys. Res. Space Physics*, 119, doi:10.1002/2013JA019305.

Liao, J., L. M. Kistler, C. G. Mouikis, B. Klecker, I. Dandouras, and J.-C. Zhang (2010), Statistical study of O^+ transport from the cusp to the lobes with Cluster CODIF data, *J. Geophys. Res., 115*, A00J15, doi:10.1029/2010JA015613.

Lockwood, M., and H. C. Carlson (1992), Production of polar cap electron density patches by transient magnetopause reconnection, Geophys. Res. Lett., 19(17), 1731-1734, doi:10.1029/92GL01993.

Lockwood, M., M. O. Chandler, J. L. Horwitz, J. H. Waite Jr., T. E. Moore, and C. R. Chappell (1985), The cleft ion fountain, *J. Geophys. Res., 90(A10),* 9736–9748, doi:10.1029/JA090iA10p09736.

McFadden, J. P. et al., (2008a), The THEMIS ESA plasma instrument and in-flight calibration, *Space Sci. Rev*.*, 141,* 277–302, doi:10.1007/s11214-008-9440-2.

McFadden, J. P., et al. (2008b), Structure of plasmaspheric plumes and their participation in magnetopause reconnection: First results from THEMIS, *Geophys. Res. Lett*., 35, L17S10, doi:10.1029/2008GL033677.

Mauk, B.H., et al. (2013), Science objectives and rationale for the Radiation Belt Storm

Probes mission, *Space Sci Rev, 179*, 3 – 27, doi: 10.1007/s11214-012-9908-y.

Mendillo, M. (2006), Storms in the ionosphere: Patterns and processes for total electron content, Rev. Geophys., 44, RG4001, doi:10.1029/2005RG000193.

Mendillo, M., M. D. Papagiannis, and J. A. Klobuchar (1970), Ionospheric storms at midlatitudes, *Radio Sci., 5*, 895–898, https://doi.org/10.1029/RS005i006p00895.

Moldwin, M. B., et al. (2003), Quantifying global plasmaspheric images with in situ observations, *Space Sci. Rev. 109*, 47 - 61, doi: 10.1007/978-94-010-0027-7_3.

Moldwin, M. B., et al. (2004), Plasmaspheric plumes: CRRES observations of enhanced density beyond the plasmapause, J. Geophys. Res., 109 (A5), A05202, doi:10.1029/2003JA010320.

Moldwin, M. B., S. Zou, and T. Heine (2016), The story of plumes: the development of a new conceptual framework for understanding magnetosphere and ionosphere coupling, Ann. Geophys., 34, 1243-1253, doi:10.5194/angeo-34-1243-2016.

Moore, T. E., *and* D. C. Delcourt (1995), The geopause, *Rev. Geophys., 33,* 175–209, *doi:*10.1029/95RG00872.

Moore, T. E., *et al.* (2008), Plasma plume circulation and impact in an MHD substorm, *J. Geophys. Res., 113,* A06219, doi:*10.1029/2008JA013050*.

Murakami, G., et al. (2013), Plasmaspheric filament: an isolated magnetic flux tube filled with dense plasmas, Geophys. Res. Lett., 40, 250–254, doi:10.1002/grl.50124.

Ober, D. M., et al. (1997), Premidnight plasmaspheric "plumes", J. Geophys. Res., 102(A6), 11325–11334, *doi:*10.1029/97JA00562.

Rideout, W. and A. Coster (2006), Automated GPS processing for global total electron content data, *GPS Solut., 10*, 219–228, doi:10.1007/s10291-006-0029-5.

Runov, A., X. J. Zhang, and V. Angelopoulos (2016), Evolution of partial ring current ion pitch angle distributions during the main phase of a storm on 17 March 2015, J. Geophys. Res. Space Physics, 121, 5284–5293, doi:10.1002/2016JA022391.

Sandel, B. R., et al. (2001), Initial results from the IMAGE Extreme Ultraviolet Imager, *Geophys. Res. Lett.,* 28, 1439-1442, doi: 10.1029/2001GL012885.

Sauvaud, J.-A., et al. (2001). Intermittent thermal plasma acceleration linked to sporadic motions of the magnetopause, first Cluster results. *Ann. Geophys.*, *19 (10/12),* 1523-1532, doi:10.5194/angeo-19-1523-2001.

Schunk, R. W., P. M. Banks, and W. J. Raitt (1976), Effects of electric fields and other processes upon the nighttime high-latitude F layer, *J. Geophys. Res., 81(19*), 3271–3282, doi:10.1029/JA081i019p03271.

Smith, P. H., and R. A. Hoffman (1974), Direct observations in the dusk hours of the characteristics of the storm time ring current particles during the beginning of magnetic storms, *J. Geophys. Res*., *79*, 966-971, doi: 10.1029/JA079i007p00966.

Strom, S. R., and G. Iwanaga (2005), Overview and history of the Defense Meteorological Satellite Program, Crosslink, 6(1), 11–15.

Su, Y.-J., et al. (2000), Plasmaspheric material at the reconnecting magnetopause, *J. Geophys. Res*., 105, 7591-7600, doi: 10.1029/1999JA000266.

Su, Y.-J., et al. (2001a), A linkage between polar patches and plasmaspheric drainage plumes, Geophys. Res. Lett., 28, 111–113, doi: 10.1029/2000GL012042.

Su, Y.-J., et al. (2001b), Plasmaspheric material on high-latitude open field lines, *J. Geophys. Res., 106(A4),* 6085–6095, doi:10.1029/2000JA003008.

Summers, D., B. Ni, and N. P. Meredith (2007), Timescales for radiation belt electron acceleration and loss due to resonant wave-particle interactions: 2. Evaluation for VLF chorus, ELF hiss, and EMIC waves, *J. Geophys. Res.,* 112, A04207, doi:10.1029/2006JA011993.

Summers, D., et al. (2008), Electron scattering by whistler-mode ELF hiss in plasmaspheric plumes, *J. Geophys. Res.* , 113, A04219, doi:10.1029/2007JA012678.

Thomas, E. G., et al. (2013), Direct observations of the role of convection electric field in the formation of a polar tongue of ionization from storm enhanced density, *J. Geophys. Res. Space Physics*, 118, 1180–1189, doi:10.1002/gra.50116.

Toledo-Redondo, S., et al. (2015), Modification of the Hall physics in magnetic reconnection due to cold ions at the Earth's magnetopause, *Geophys. Res. Lett*., 42, 6146–6154, doi:10.1002/2015GL065129.

Tsyganenko, N. A. and M. I. Sitnov (2005), Modeling the dynamics of the inner magnetosphere during strong geomagnetic storms, J. Geophys. Res., v. 110 (A3), A03208, doi: 10.1029/2004JA010798.

Tu, J.-N., et al. (2007), Extreme polar cap density enhancements along magnetic field lines during an intense geomagnetic storm, J. Geophys. Res., 112, A05201, doi:10.1029/2006JA012034.

Wang, S., et al. (2014), Hot magnetospheric O^+ and cold ion behavior in magnetopause reconnection: Cluster observations, *J. Geophys. Res. Space Physics*, 119, 9601-9623, doi:10.1002/2014JA020402.

Walsh, B. M., et al. (2013), Statistical analysis of the plasmaspheric plume at the magnetopause, *J. Geophys. Res. Space Physics*, 118, 4844-4851, doi:10.1002/jgra.50458.

Walsh, B. M., et al. (2014a), The plasmaspheric plume and magnetopause reconnection, *Geophys. Res. Lett.,* 41, 223-228, doi:10.1002/2013GL058802.

Walsh, B. M., et al. (2014b), Simultaneous ground and space-based observations of the plasmaspheric plume and magnetospheric reconnection, *Science*, 343/6175, 1122-1125, doi: 10.1126/science.1247212.

Weber, E. J., et al. (1984), F layer ionization patches in the polar cap, *J. Geophys. Res*., 89, 1683-1694, doi: 10.1029/JA089iA03p01683.

Whitteker, J.H., et al. (1976), Snapshot of polar ionosphere, *Planet. Sp. Sci*., 24/1, 25-32, doi: 10.1016/0032-0633(76)90057-X.

Wygant, J. R., et al. (2013), The Electric Field and Waves (EFW) instruments on the

Radiation Belt Storm Probes Mission, *Space Science Review*, 183-220, doi: 10.1007/s1124-013-0013-7.

Yeh, H.-C., and J. C. Foster (1990), Storm-Time Heavy Ion Outflow at Mid-Latitudes, *J. Geophys. Res., 95,* 7881-7891, doi: 10.1029/JA095iA06p07881.

Yuan, Z.-G., X.-H. Deng, and J.-F. Wang (2008), DMSP/GPS observations of intense ion upflow in the midnight polar ionosphere associated with the SED plume during a super geomagnetic storm, *Geophys. Res. Lett*., 35, L19110, doi:10.1029/2008GL035462.

Yuan, Z.-G., et al. (2009), F region behavior in the SED plume during a geomagnetic superstorm: A case study, *J. Geophys. Res*., 114, A08303, doi:10.1029/2008JA013841.

Yuan, Z., et al. (2012a), Wave-particle interaction in a plasmaspheric plume observed by a Cluster satellite, *J. Geophys. Res.*, 117, A03205, doi:10.1029/2011JA017152.

Yuan, Z., et al. (2012b), Characteristics of precipitating energetic ions/electrons associated with the wave-particle interaction in the plasmaspheric plume, *J. Geophys. Res*., 117, A08324, doi:10.1029/2012JA017783

Zeng, W., and J. L. Horwitz (2008), Storm enhanced densities (SED) as possible sources for Cleft Ion Fountain dayside ionospheric outflows, Geophys. Res. Lett., 35, L04103, doi:10.1029/2007GL032511.

Zhang, Q. H., et al. (2013a), Direct observations of the evolution of polar cap ionization patches, *Science*, 339 (6127), 1597-1600, doi:10.1126/science.1231487.

Zhang Q. –H., et al. (2013b), Polar cap patch segmentation of the tongue of ionization in the morning convection cell, *Geophys. Res. Lett.*, 40, 2918–2922, doi:10.1002_grl.50616.

Zhang, Q.-H., et al. (2015), Direct observations of the full Dungey convection cycle in the polar ionosphere for southward interplanetary magnetic field conditions. *J. Geophys. Res. Space Phys*, *120*, 4519–4530. doi: 10.1002/2015JA021172.

Zhang, Q.-H., et al. (2016), Polar cap patch transportation beyond the classic scenario, *J. Geophys. Res. Space Physics*, 121, 9063–9074, doi:10.1002/ 2016JA022443.

Zhang Q. -H., et al. (2018), Observations of the step-like accelerating processes of cold ions in the reconnection layer at the dayside magnetopause, *Science Bulletin*, 63 (1), 31-37, doi: 10.1016/j.scib.2018.01.003.

Zou, S., et al. (2013), Multi-instrument observations of SED during 24–25 October 2011 storm: Implications for SED formation processes, *J. Geophys. Res. Space Physics,* 118, 7798–7809, doi:10.1002/2013JA018860.

TABLES

Table 1. Simultaneous Observations of Plume Characteristics

Instrument	Location	Altitude	Velocity	Density	Plasma Flux
Millstone Hill	Noon Cusp	450 km	~ 1000 m/s	~ 3.e11 m^{-3}	~ 3.e14 $m^{-2}s^{-1}$
DMSP	SAPS 19 MLT	840 km	~ 1700 m/s	~ 3.e11 m^{-3}	~ 4.e14 $m^{-2}s^{-1}$
DMSP	Polar TOI	840 km	~ -500 m/s	~ 1.e11 m^{-3}	~ 5.e13 $m^{-2}s^{-1}$
RBSP-A	SAPS 19 MLT	3 R_E	~ 7000 m/s	~ 1.e8 m^{-3}	~ 7.e11 $m^{-2}s^{-1}$
THEMIS-A	Plume 12 MLT	5 R_E	~ 4.e4 m/s	~ 2.5e8 m^{-3}	~ 1.e13 $m^{-2}s^{-1}$
THEMIS ESA	Exhaust Jet	6 R_E	~ 3.e5 m/s	~ 3.e7 m^{-3}	~ 1.e13 $m^{-2}s^{-1}$

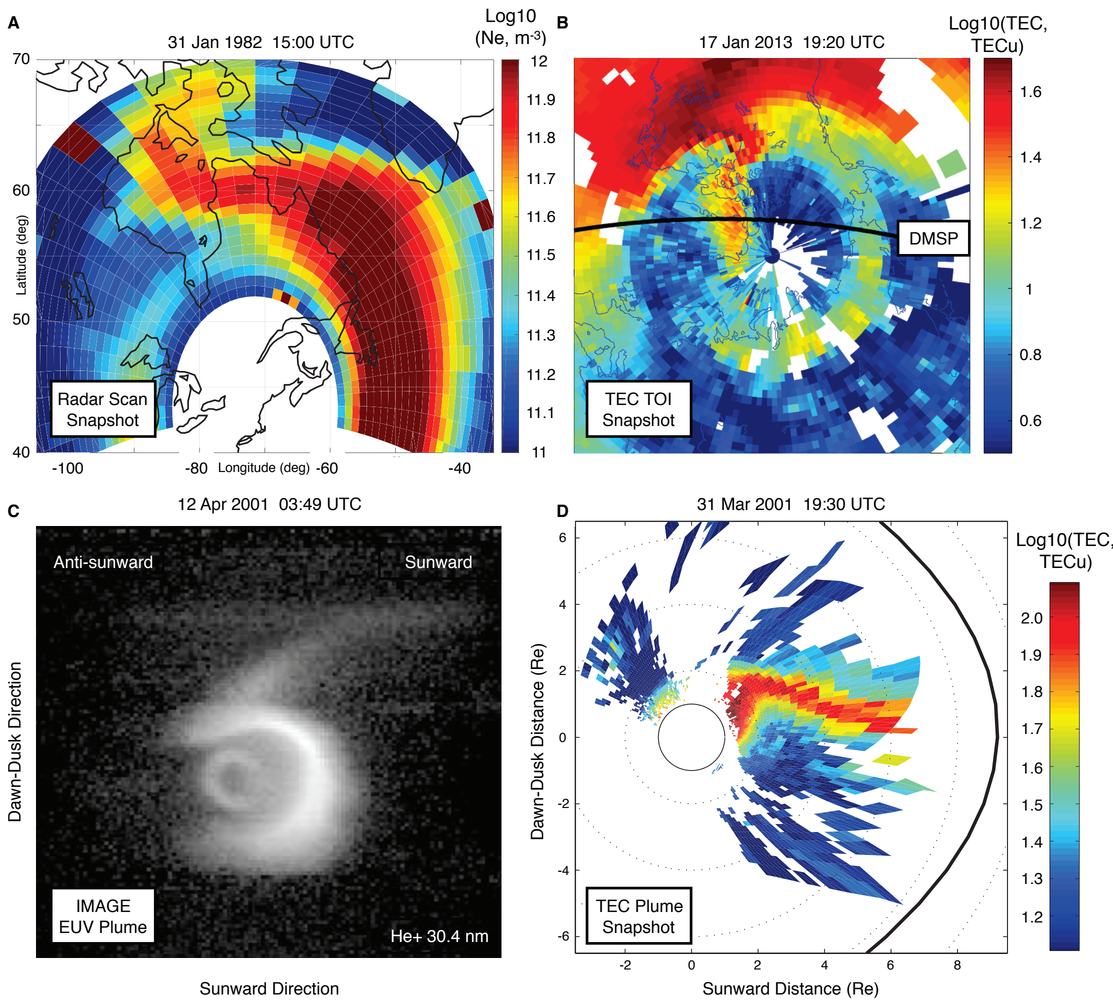

Figure 1. (A) Azimuth scan observations with the Millstone Hill radar provide a spatial "snapshot" of a continuous stream of plasma carried from low latitudes in the evening sector to the cusp and polar cap. The observations of ionospheric electron density were made over a ~30-minute interval near the noon meridian and are plotted in latitude//longitude coordinates with north at the top. (B) Aggregation of 5 minutes of northern hemisphere GPS TEC observations provided global imagery of a nearly-identical feature some 30+ years later during a January 2013 storm. The TEC data are presented in polar local time geodetic coordinates with noon at the top for latitudes above 30 N. The plume extending poleward from North America is seen to stretch anti-sunward across polar latitudes and to merge into the auroral oval in the midnight sector. The orbital track of a DMSP satellite crossing polar latitudes is shown as a black line. (C) Space based imagery of the outer extent of the plasmasphere depicts the erosion and sunward extension of the cold plasma plume. An IMAGE EUV snapshot looking down on the plasmasphere and plume from above north polar latitudes is shown (the Sun is to the right). (D) GPS TEC observations, when mapped along the magnetic field into the magnetospheric equatorial plane (the Sun is to the right), reveal plasma boundaries closely reproducing the evolution of the geospace plume at magnetospheric heights, indicating its full sunward extension toward the magnetopause (black line).

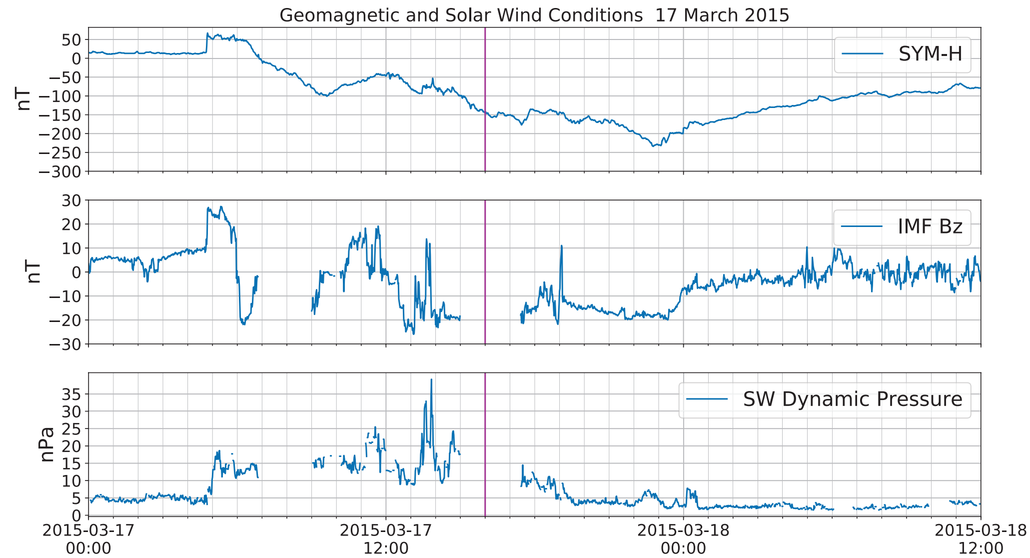

Figure 2. Geomagnetic and solar wind conditions during 17-18 March 2015 from 1-min cadence observations in the NOAA OMNI database. A solar wind shock and storm sudden commencement at ~04:45 UTC on 17 March was followed by a main storm phase with peak at < -220 nT near 23:00 UTC and a subsequent recovery period. The magenta line indicates the time of the near-simultaneous observations of the geospace plume examined in detail in this study (~16:00 UTC on 17 March).

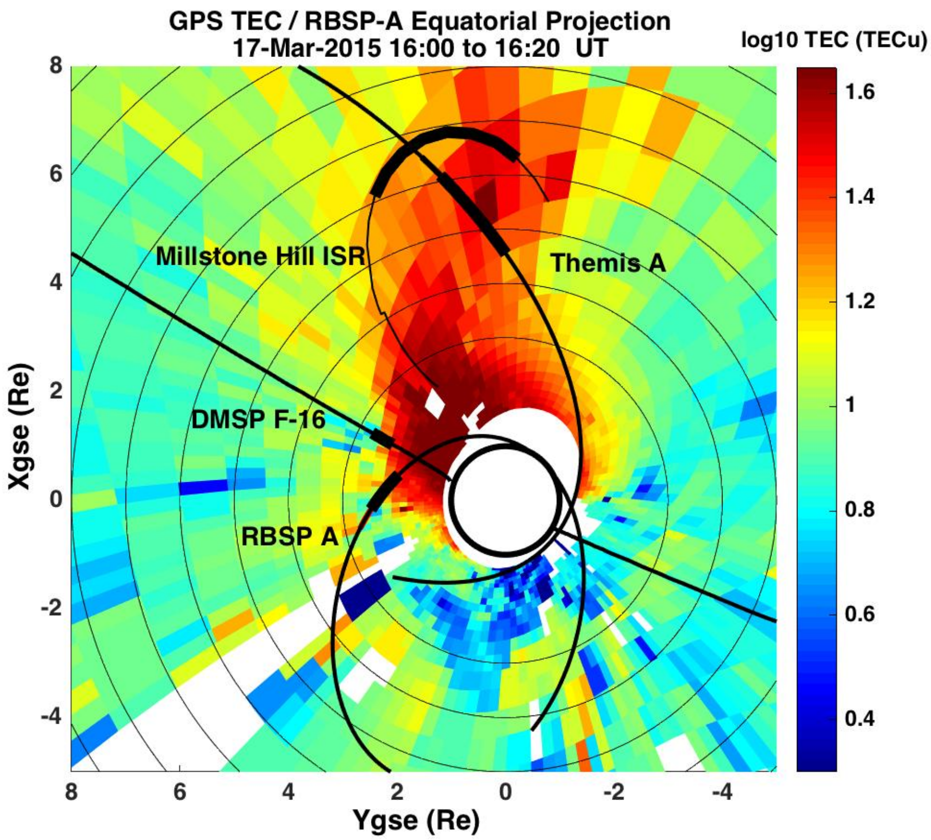

Figure 3. Orbits and observing locations for low and high-altitude instruments early in the 17 March 2015 event are projected onto the magnetospheric equatorial plane in X-Y GSE coordinates (Sun at the top). Their relationship to the evolving geospace plume structure is described by equatorially mapped northern hemisphere GPS TEC observations. Heavy shading denotes the extent of geospace plume observations along each orbit/observation path.

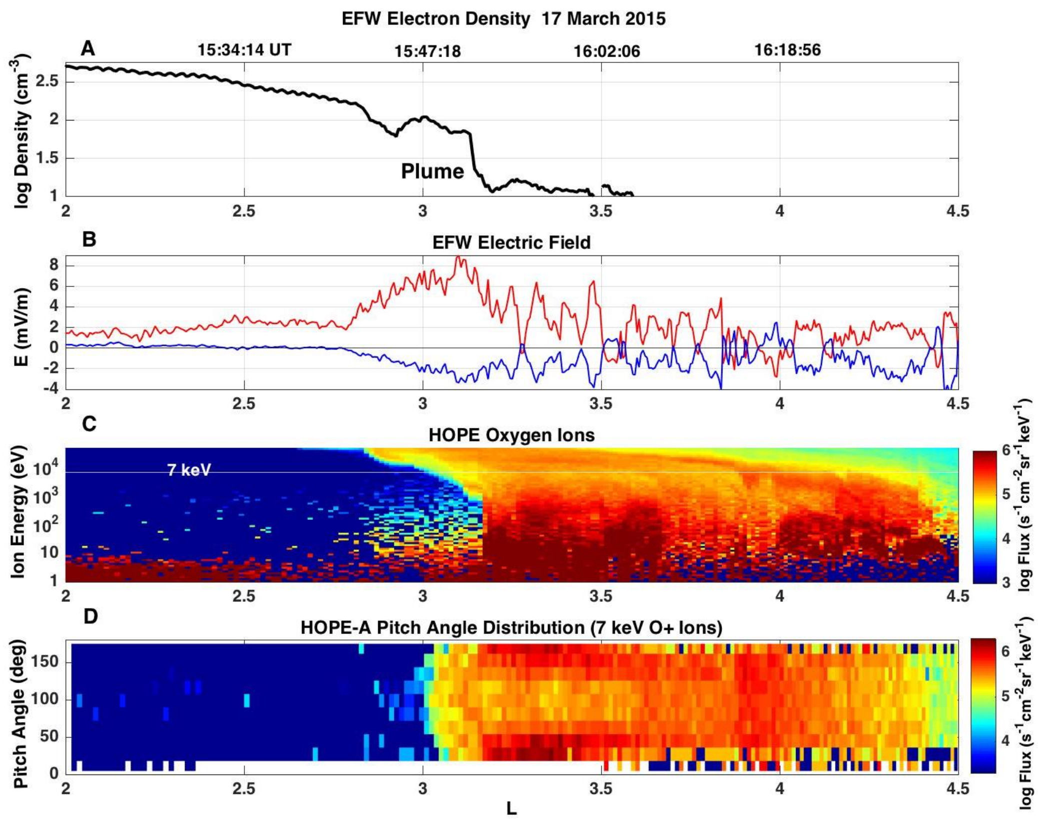

Figure 4. The relationship of the SAPS, the ring current, and the geospace plume were observed by Van Allen Probe A as its near-equatorial outbound orbit crossed the plasmasphere boundary layer at 18 MLT. (A) In situ plasma density observations (EFW boom potential technique) identified the plume near its point of formation near L ~ 3 (15:45 UT). (B) Strong radially outward electric fields (EFW; red curve; azimuthal component is shown in blue) were observed across the SAPS flow channel responsible for the sunward advection of outer plasmaspheric ions in the geospace plume. (C) A 'nose' of hot ring current O^+ ions observed with the HOPE instruments extended across the region of SAPS electric field. (D) Bi-directional field aligned fluxes characterized the HOPE O^+ pitch angle distributions at energies up to ~ 10 keV immediately adjacent to the outer extent of the geospace plume.

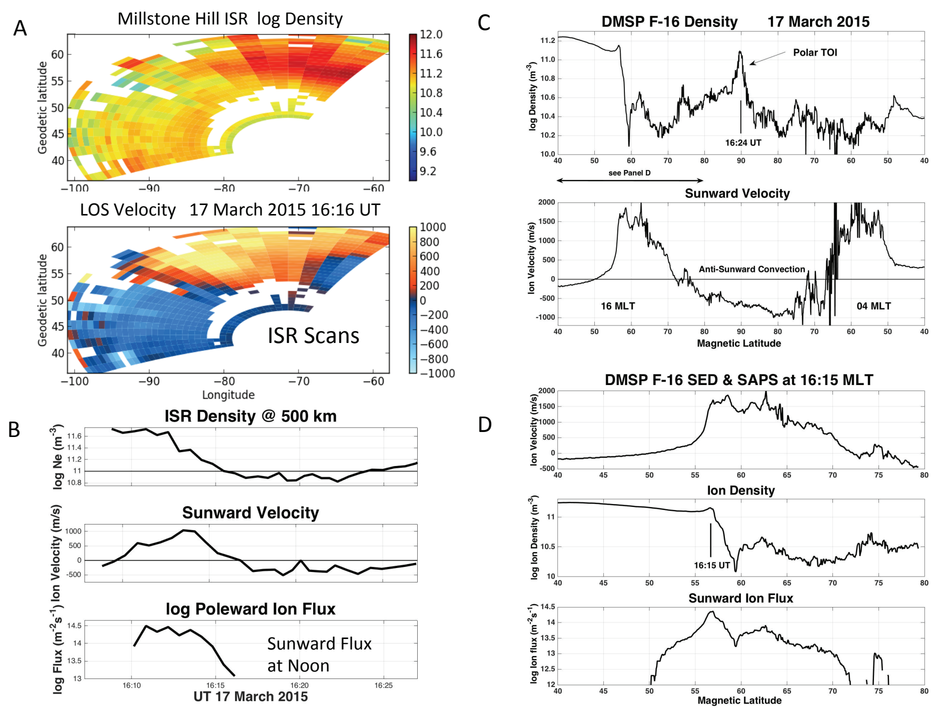

Figure 5. Radar and LEO observations depict the geospace plume at ionospheric heights.

(A) Similar to the case described in Figure 1A, Millstone Hill radar scans to the north and west made simultaneous observations of high plasma densities and strong poleward velocities associated with plume and SAPS flow through the noontime cusp. (B) Radar observations of F-region O^+ density and line of sight (LOS) velocity across the noon sector determined the ion flux to the cusp at 500 km altitude to be > $3.x10^{14}$ m^{-2} s^{-1}. (C) In situ ion density (upper panel) and cross-track ion velocity (positive sunward) were observed by DMSP F-16 across auroral and polar latitudes along a dusk-dawn orbit similar to that shown in Figure 1B. The polar tongue of ionization (TOI) was encountered at 16:24 UT near 90 deg latitude embedded in the cross polar cap antisunward flow. (D) DMSP F-16 crossed the SAPS flow channel between 55 and 58 deg magnetic latitude at 16 MLT. Storm enhanced density (57 deg; middle panel) embedded in the SAPS flow marked the equatorward edge of the ionospheric trough. Sunward topside O^+ ion flux of ~ 2.5 $x10^{14}$ m^{-2} s^{-1} (bottom panel) was observed associated with the SAPS/SED flow.

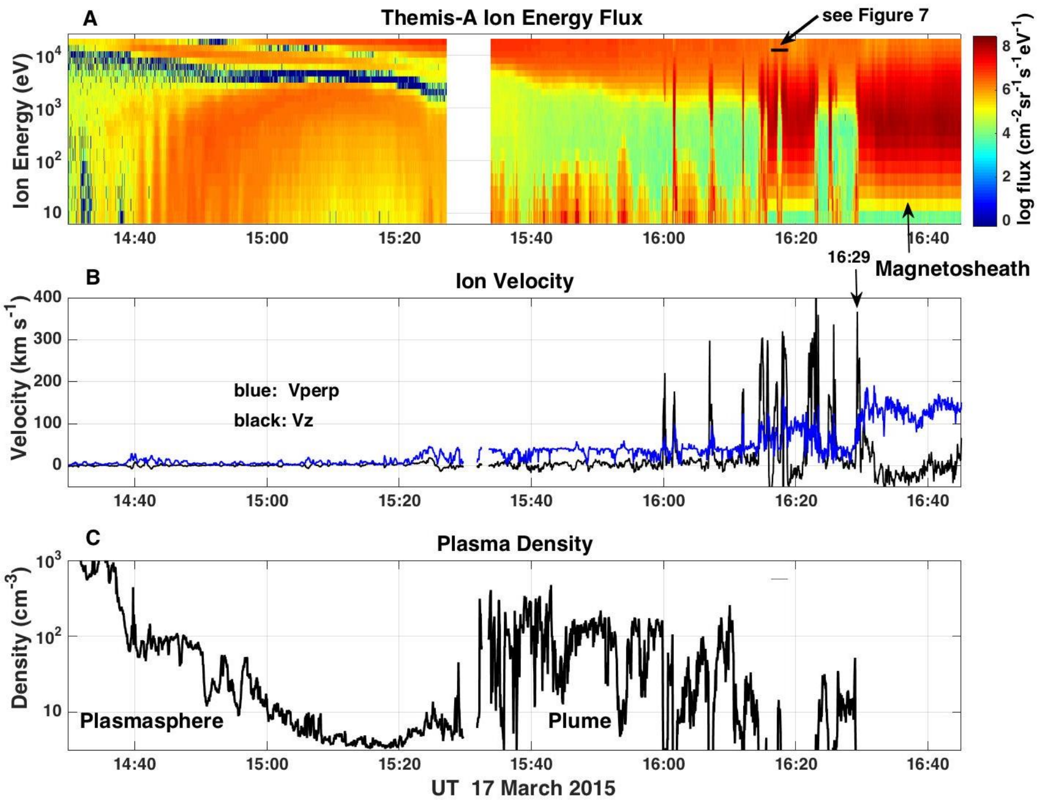

Figure 6. THEMIS-A exited the plasmasphere near ~14:40 UT and flew into high-density plume plasma for the one hour interval ~15:30 UT – 16:30 UT. Magnetopause reconnection signatures were observed after ~ 16:00 UT and the magnetosheath beyond the reconnection region was entered shortly after 16:30 UT. (A) The ESA spectrogram of total ion energy flux between 6 eV and 25 keV observed the characteristics of these regions (see text). The extent of the region shown in detail in Figure 7 is indicated. (B) ESA ion velocity measurements spanned the region of the plume (~ 40 km/s) and identify the regions of active reconnection through the appearance of strong + Vz exhaust jets (> 100 km/s). (C) The in situ electron density profile calculated from THEMIS -A spacecraft potential clearly defines the extent and intensity of the dayside geospace plume plasma.

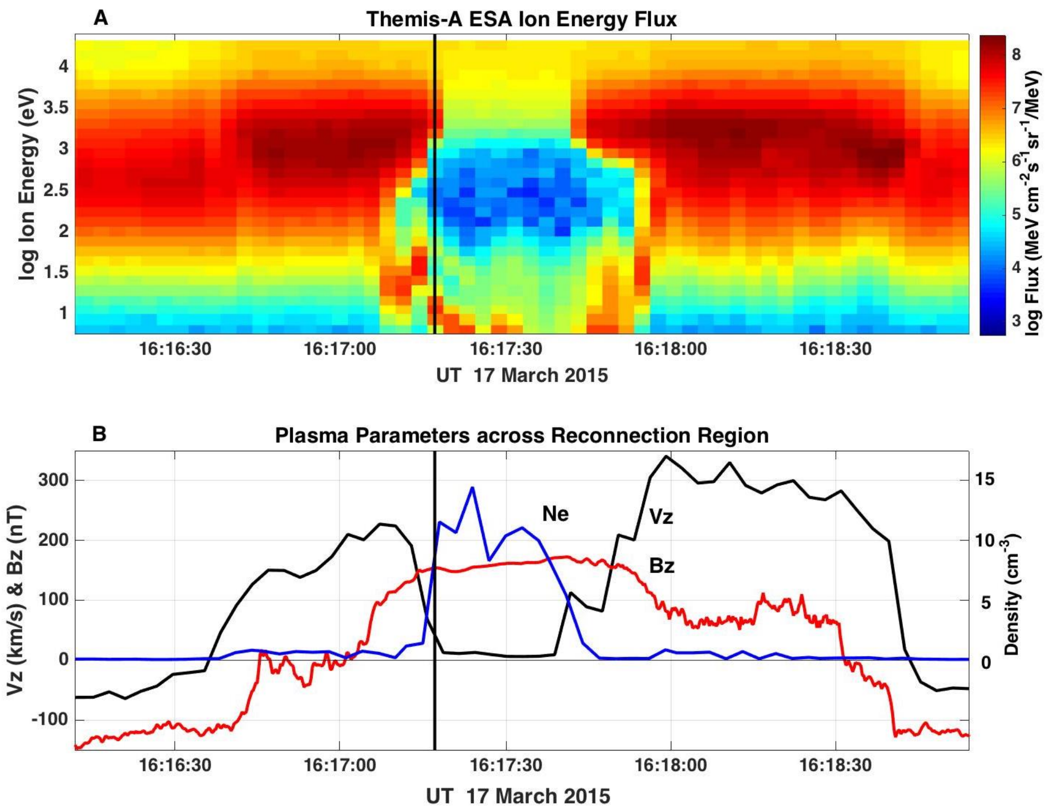

Figure 7. THEMIS-A observed multiple intersections with regions of active reconnection. (A) An ESA burst mode ion energy flux spectrogram is shown for a ~ 3 min interval as the fluctuating magnetopause position carried the merging region back and forth over the outbound spacecraft. A pronounced low energy population with center energy ranging from <5 eV to ~50 eV was observed between 16:17:00 UT and 16:18:00 UT. A black vertical line marks 16:17:15 UT (cf. Figure 9).
(B) Observed cold plasma density (blue), Z_{GSM} component of the magnetic field (red), and field aligned velocity (black; Vz) are shown. Large high speed flows (Vz) identify the reconnection jets. High cold plasma density, positive B_Z, and small V_Z characterize the magnetosphere immediately adjacent to the reconnection region.

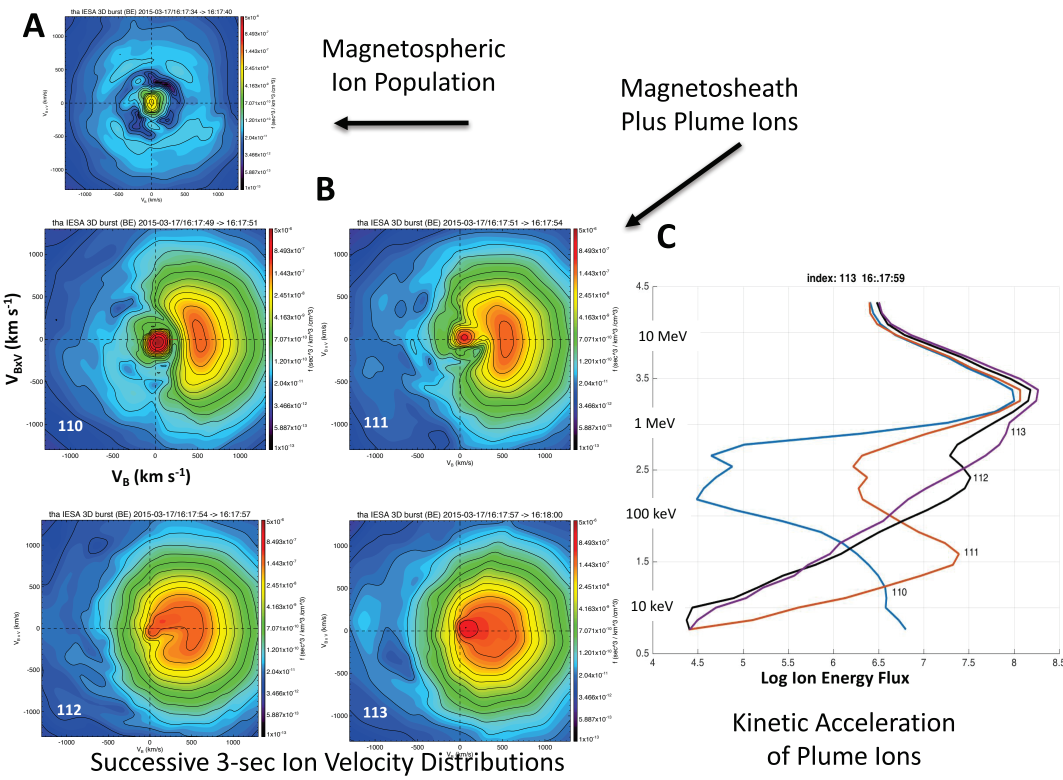

Figure 8. THEMIS-A ESA ion velocity distributions and energy spectra are shown for the magnetopause crossing recorded between 16:17:40 UT and 16:18:00 UT (cf. Figure 7).
(A) The velocity distribution of magnetospheric ions immediately adjacent to the magnetopause is shown. A weak flux of the cold ions was seen above detector threshold around zero energy.
(B) Successive 3-s velocity distributions observed as THEMIS-A approached the magnetopause and the merging region show that a portion of the cold population was progressively kinetically accelerated to > 300 eV energy as the exhaust jet was approached. "D-shaped" ion distributions representative of magnetosheath particles were observed. The larger gyroradii of the more energetic ions results in their incursion onto field lines associated with the guiding centers of the adjacent colder population.
(C) Progressively increasing peak energies of the low energy ions at times corresponding to the 4 distributions shown in panel B correspond to the kinetic energies of H+ ions for the observed values of V_Z as shown in Figure 7.

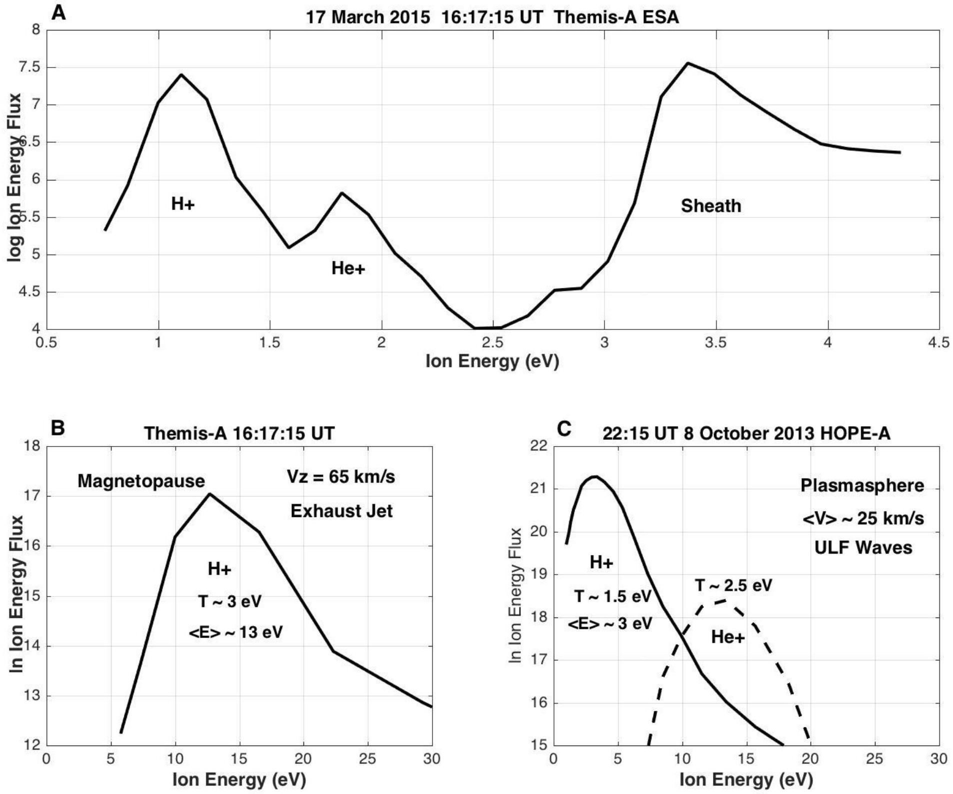

Figure 9. A THEMIS-A ESA one-dimensional ion energy distribution cutting across the low energy population at 16:17:15 UT is shown (see Figure 7 for the spatial location of this measurement). The difference of kinetic energies for cold ion species accelerated in the reconnection velocity field produces clearly separated H+ and He+ energy peaks. As seen in the ion spectrogram of Figure 7, magnetosheath ions are observed separately at energies > 2 keV.
(B) The temperature of the cold H+ population in the 17 March 2015 event was found to be ~3 eV, as calculated from the energy spread of its 1-D distribution (see text).
(C) The temperature of the H+ ions at the merging region is consistent with other measurements of ion temperatures in the outer plasmasphere. Spectral widths of H+ and He+ ions accelerated kinetically to energies > 2 eV by strong ULF waves were observed well inside the plasmapause by the HOPE instrument on RBSP-A during the 8 October 2013 shock event. The outer plasmaspheric H+ and He+ temperatures (1.5 eV and 2.5 eV) observed are fully consistent with the temperature of the low energy plume ion population described in Panel B.